

Enhancing the analysis of murine neonatal ultrasonic vocalizations: Development, evaluation, and application of different mathematical models

Rudolf Herdt,¹ Louisa Kinzel,¹ Johann Georg Maaß,^{2,3, a} Marvin Walther,¹ Henning Fröhlich,² Tim Schubert,² Peter Maass,¹ and Christian Patrick Schaaf²

¹Center for Industrial Mathematics, University of Bremen, Bremen 28334, Germany

²Institute of Human Genetics, University of Heidelberg, Heidelberg 69120, Germany

³Also at: Interdisciplinary Neurobehavioral Core, University of Heidelberg, Heidelberg, 69120, Germany

Rodents employ a broad spectrum of ultrasonic vocalizations (USVs) for social communication. As these vocalizations offer valuable insights into affective states, social interactions, and developmental stages of animals, various deep learning approaches have aimed to automate both the quantitative (detection) and qualitative (classification) analysis of USVs. Here, we present the first systematic evaluation of different types of neural networks for USV classification. We assessed various feedforward networks, including a custom-built, fully-connected network and convolutional neural network, different residual neural networks (ResNets), an EfficientNet, and a Vision Transformer (ViT). Paired with a refined, entropy-based detection algorithm (achieving recall of 94.9 % and precision of 99.3 %), the best architecture (achieving 86.79 % accuracy) was integrated into a fully automated pipeline capable of analyzing extensive USV datasets with high reliability. Additionally, users can specify an individual minimum accuracy threshold based on their research needs. In this semi-automated setup, the pipeline selectively classifies calls with high pseudo-probability, leaving the rest for manual inspection. Our study focuses exclusively on neonatal USVs. As part of an ongoing phenotyping study, our pipeline has proven to be a valuable tool for identifying key differences in USVs produced by mice with autism-like behaviors.

Pages: 1–18

I. INTRODUCTION

Ultrasonic vocalizations (USVs) in rodents are calls above our hearing range (>20 kHz) which are produced by rodents and play an important role in the social interaction of the animals. Mice, in particular, emit a rich variety of USVs that differ in length, frequency, and modulation. Both the quantity and quality of these calls can provide insights into well-being, development, and sociability.^{1–3} The vocalizations of mice evolve throughout development, following an ontogenetic profile.⁴ Anomalies in USVs have been described in genetic mouse models for autism, schizophrenia, and Down syndrome.^{5–7} Due to its high informative value, investigation of call behavior has sparked research interest and has been established as a reliable tool in behavioral neuroscience and pharmacology.⁸

While the recording of USVs is a simple and fast procedure, until now, analyzing the recordings has been very labor-intensive, thereby restricting the scientific potential of the experiment. Conventional manual quantification (call detection) and qualitative analysis (call

classification) can take up to 2 hours for a 5-minute-long recording. In addition, manually analyzed datasets show low interrater reliability.

New mathematical deep learning models now make it possible to both detect and classify calls, hence speeding up the process and improving the reliability significantly. So far, most efforts have focused on automating the analysis of USVs emitted by rats or adult mice in the context of both affective and aversive states.^{9,10} In this paper, we focus specifically on neonatal USVs produced upon separation from the litter.

Studying neonatal USVs in mice offers a unique opportunity to investigate the early developmental aspects of acoustic communication deficits and provides valuable insights into the underlying mechanisms of autism-like behavior.¹¹ Pups separated from the mother will produce a large quantity and variety of USVs in order to elicit retrieval by the mother.¹² Quantifying and classifying these calls are the subject of many neurobehavioral studies. The diverse nature of the calls combined with inevitable background noise complicates the analysis. Even previous advanced models, as reviewed by Pessoa et al. in 2022, face challenges in achieving high values for both recall and precision.¹⁰ The subsequent classification of neonatal USVs is especially difficult as the distribution

^ajohann.maass@med.uni-heidelberg.de

of calls changes over time.² Different groups have tried to use a variety of mathematical models and forms of neural networks (threshold-based, fully connected, CNN, recurrent, etc.) to detect and classify calls.^{9,10,13–15} But different types of data require different types of algorithms. And the question of which network type is best used for the classification of calls is yet to be answered.

It was our goal to develop a fully automated pipeline for the analysis of neonatal USVs. In the first step, we developed an algorithm that can reliably detect USVs in recordings. For the subsequent classification, we built and tested different types of neural networks to determine which network is best suited for the task. In the end, the algorithms for the detection and the classification were concatenated to a comprehensive pipeline that can automatically quantify and classify calls in recordings of pups, using advanced mathematical models.

In this paper, we present the first systematic evaluation of different neural networks for USV classification. We also analyze the network structure in depth to understand which features drive the decision-making progress and to increase the acceptance and understanding of AI-driven decisions.

Finally, we analyzed USV data from an ongoing phenotypization project and were able to demonstrate the efficacy of the algorithm. Our pipeline improves the overall accuracy of the analysis and provides valuable insights into the distinct ways various deep learning models handle acoustic data.

II. MATERIAL

A. Signal acquisition setup

Recordings were made using an UltraSoundGate condenser microphone (CM16/CMPA, Avisoft Bioacoustics) connected to a computer via an Avisoft UltraSoundGate USG416H audio device. The USV signals were recorded using Avisoft-RECORDER software (Avisoft Bioacoustics) at a sampling rate of 250 kHz and stored in WAV file format. The microphone was positioned close to the ceiling of a 42x42x42 cm wide sound-attenuating cube, 30 cm above the ground. The room temperature was set to 22°C, and the experimenter ensured that there were no disturbing noises.

B. Dataset

We used USV recordings from an ongoing phenotypization study comparing three heterozygous mouse lines harboring different pathogenic variants in *Nr2f1*. The gene encodes for a transcription factor that plays an important role in neurogenesis.¹⁶ In humans, pathogenic variants in *NR2F1* are associated with intellectual disability, developmental delay, and autism.¹⁷ Preliminary behavioral data revealed that mice harboring a pathogenic variant in *Nr2f1* resemble the human phenotype, including autism-like behavior, as shown by a strongly reduced number of USVs during pup separation

as well as asocial behavior in the three-chamber test (unpublished data). All lines have a C57BL/6J background, as Peleh et al. have shown that the background is suitable for the analysis of USVs in pups.²

The animals were housed at the Interdisciplinary Neurobehavioral Core (INBC) of Heidelberg University on a 12-hour dark-light cycle. They had ad libitum access to food and water throughout the experiments. Tests were always conducted at the same time. Recordings were made at three different postnatal (P) ages: P4, P8, and P12. We included both males and females. At P2, animals were tattooed for identification.

Testing of all three lines at the respective timepoints created a dataset comprising a total of 593 recordings (5 min. each), with a total of 160,295 calls (as evaluated by our detection algorithm).

We utilized five distinct datasets in our study:

1. 593-Dataset: This comprises the entirety of 593 recordings and serves as the foundational pool from which the subsequent datasets are derived.

2. D-Dataset: Consists of manually detected calls in a total of 30 recordings and was used for building the detection algorithm.

3. VD-Dataset: Encompasses 6 additional manually detected recordings used for validating the detection algorithm.

4. M-Dataset: Consists of 13 manually detected recordings (from the D-Dataset) that were subsequently manually classified.

5. A-Dataset: Comprises 16 recordings that were automatically detected using the previously established algorithm, followed by manual classification.

Manual detection and classification were conducted using SASLabPro Avisoft (Avisoft Bioacoustics). The detection algorithm development relied on D-Dataset and VD-Dataset, while M- and A-Dataset were used for the classification task. For information on the distribution of call classes in the datasets see Table I.

Upon completing the pipeline, the entire 593-Dataset was analyzed.

C. Syllable classes

We adopted the call categories outlined by Scattoni et al. (2008), further refined by Grimsley et al. (2011), and extensively examined by Peleh et al. (2019), as the latter study was also conducted at the INBC.^{2,3,18} Building on these categories, we consolidated similar classes based on our own observations. This consolidation aimed to augment the number of calls per category, thereby bolstering the reliability of our tests. Specifically, we grouped calls featuring two or more simultaneous frequencies (harmonics and composite), calls exhibiting an absolute modulation of frequency exceeding 6 kHz (complex, chevron, upward, and downward), and calls involving a frequency change with no temporal interruption (two-syllable and frequency step). When combined with short calls and those with a constant frequency, this results in a total of five categories:

TABLE I. Call class distribution in the automatically (A) and manually (M) detected dataset.

Dataset	size	constant frequency	modulated frequency	frequency step	simultaneous frequencies	short
A-Data	2013	261 (12.97%)	882 (43.82%)	304 (15.10%)	165 (8.20%)	401 (19.92%)
M-Data	2562	501 (19.56%)	760 (29.66%)	480 (18.74%)	119 (4.64%)	702 (27.40%)

- **Class 1 Flat:** Calls with a modulation in frequency <6 kHz.
- **Class 2 Modulated:** Calls with a modulation in frequency >6 kHz.
- **Class 3 Frequency Step:** Calls with an instantaneous frequency change without any interruption in time.
- **Class 4 Composite:** Calls with two harmonically independent components emitted simultaneously.
- **Class 5 Short:** Calls with a duration <5 ms.

Examples for each class can be seen in [Figure 1](#). Whereas most calls can be easily classified, some are indistinguishable as they fall on the verge between two definitions. Such calls were not included in Datasets M and A.

The pooling was particularly crucial, given that the relative distribution of calls by category emitted by the pups evolves through development and some classes (i.e., two-syllable or chevron) have a significantly lower relative distribution in pups compared to adolescent animals.² Also, some classes only account for a small fraction of calls. For example, all harmonics, two-syllable, and composite calls together account for less than 10 % of the USVs in C57BL/6J pups.³ We have pooled call categories that show a similar resemblance to ensure that each category was based on a sufficiently large dataset. Analysis conducted later indicated that pooling did not impede the identification of subtle differences in the quality of USV calls.

III. METHODS

A. Structure of the pipeline

Our final goal is to develop a data processing pipeline which allows to load a USV recording and which returns a complete list of calls in this recording along with their classification. Our segmentation and classification code is accessible online through this [GitHub](#) repository. [Figure 2](#) illustrates the comprehensive methodological pipeline.

The two basic building blocks of this pipeline are aimed at 1) extracting short acoustic signals containing only a single call (detection) followed by an analysis block aimed at 2) characterizing the type of call (classification).

Finally, these findings are combined in a list of calls along with their classification and returned to the user.

When describing these two blocks in more detail, we have to distinguish between a) the development and b) the application phase of the pipeline. The application phase uses a simple pipeline as depicted in [Figure 2](#). In principle, we would like to have software capable of analyzing 100 % of all datasets with 100 % accuracy. However, this is unrealistic in a laboratory setting where different people might conduct experiments, various instruments may be used for recording, and background noise can significantly differ. Therefore, we aim for software that automatically determines a confidence measure for the data. If the confidence is acceptable, we expect reliable classification; if not, the data is flagged for manual inspection. We summarize this approach by defining the *80-90 challenge*. i.e. we aim at automatically analyzing at least 80 % of all calls with an accuracy of at least 90 %. This would result in a reduction of the manual workload by a factor of 5. Furthermore, it allows users to define a minimum level of accuracy tailored to the specific research question. This translates into a threshold that separates calls into those that can be automatically analyzed with the defined accuracy and those that require manual inspection.

During the development phase of the software, we also want to analyze and compare different concepts. The concepts used for the detection block are linear in the sense that we use a natural pipeline and develop criteria for optimizing individual steps. For the development of the subsequent classification block, we have primarily used machine learning techniques from deep learning and we have tested several network architectures. For each architecture we need to specify its hyperparameters, suitable data preprocessing and its output parameters used for evaluating its performance. After training of the pipeline, we face the common problem of machine learning, that the structures used by the algorithm for reaching its decision on particular classifications are hidden in the trained network parameters. As an additional feature of our paper, we also aim at visualizing features used by the algorithm in a way that is accessible to human users.

B. Segmentation, detection

The first step in our workflow is the detection of individual ultrasonic vocalizations as depicted in [Figure 3](#). In principle, each recording has to be segmented into pe-

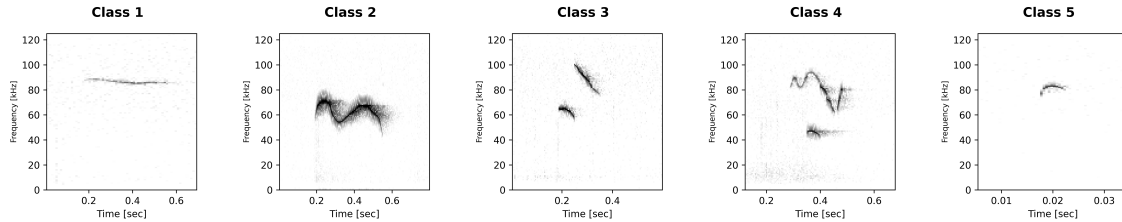


FIG. 1. Overview of the 5 classes.

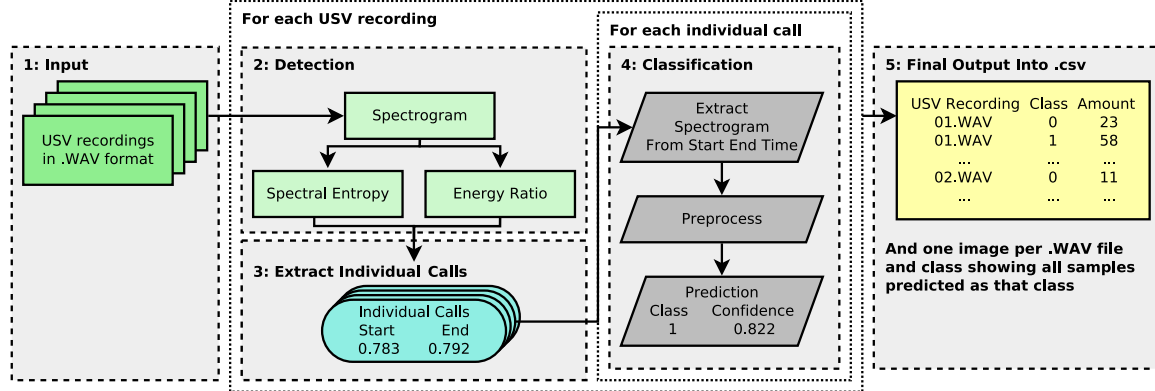


FIG. 2. Overview of the final pipeline.

riods of vocalization and silence. It is important to note that complete silence is difficult to achieve, and a varying level of background noise cannot be avoided.

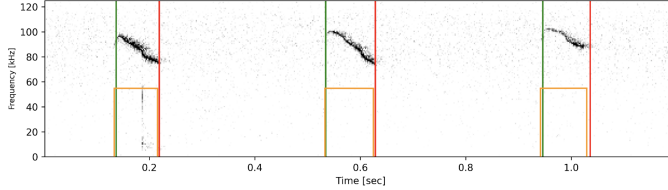


FIG. 3. A spectrogram displaying three calls, annotated by both the automatic detection (green and red vertical lines) and the manual detection (orange horizontal line). (Color online)

In order to access discriminating features more easily, the original measurement, i.e., the acoustic pressure wave recorded by the microphone, is converted into a spectrogram. A spectrogram $S(t, f)$ depicts the active frequencies f for each point in time t . For a general introduction to spectrograms, one can consult the textbook by Oppenheim on signal processing.¹⁹

In our analysis, the spectrogram representation is computed by a short-term Fourier transform (STFT) using a Tukey window with a shape parameter of 0.25, a segment length of 256, and a discrete Fourier transform

of length 256 with no overlap. This results in a temporal resolution of slightly more than 1 ms.

Taking the square of the STFT values then yields the energy spectrogram $S(t, f)$. The detection algorithm relies on the definition of features of $S(t, f)$ that enable precise determination of the moment a vocalization starts and ends.

Our main feature is spectral entropy. As a measure of the power distribution in the frequency domain, entropy enables differentiation between vocalizations and noise at each time step in the spectrogram. Vocalizations generally only have energy in a very narrow frequency band (low entropy), while noise generally has a dispersed energy spectrum (high entropy). As background noise is generally restricted to frequencies below 40 kHz, we compute the spectral entropy in the range between 40 and 110 kHz in order to discard low-frequency noise (e.g., mouse movements). We call this restricted part of the spectrogram $S^h(t, f)$, where t ranges in discrete time steps between 0 and the length of the recording, and f ranges in discrete frequency steps between 40 and 110 kHz. Then the spectral entropy $H(t)$ is computed by normalization.

$$P(t, f) = \frac{S^h(t, f)}{\sum_{f'} S^h(t, f')} \quad (1)$$

and the subsequent calculation of the standard entropy.

$$H(t) = - \sum_f P(t, f) \log P(t, f). \quad (2)$$

To enhance this detection, we incorporated the energy at different frequency ranges as additional features, for example.

$$E^h(t) = \sum_{f=40}^{110} S(t, f) \quad \text{or} \quad E^l(t) = \sum_{f=0}^{39} S(t, f).$$

The first value, $E^h(t)$, denotes the energy of the signal in the typical range of mouse vocalization. The second, low-frequency value, $E^l(t)$, serves as an indicator for the background noise. However, a simple threshold on these values did not significantly improve the accuracy of the detection. Better results were obtained by thresholding the ratio $R(t)$.

$$R(t) = \frac{E^h(t)}{E^l(t)}. \quad (3)$$

[Figure 4](#) illustrates the entropy and the ratio threshold. Combined, they yield an intermediate detection indicator $i(t)$, which takes a value of 0 or 1 for each time t , indicating whether the spectral entropy as well as the energy ratios are above or below the threshold. In our experiments, we fixed the threshold to 3.5, and a 1 was assigned to $i(t)$ if $H(t) \leq T_H$ and $R(t) \geq T_R$.

Subsequently, we fuse very short gaps in the detection, which sometimes occur toward the quieter end of a vocalization, and we delete very short detections since they are likely noise. For this purpose, we define two parameters N_g and N_d and fuse gaps if they are shorter than N_g time steps, and delete detections completely if they are shorter than N_d time steps. The final output is a list of start and end points of all vocalizations in a recording.

After fixing the parameters of the algorithm, we evaluated its performance on 6 recordings, i.e., 30 min. of USV measurements, which were not used in the development of the algorithm. Manual annotation resulted in a set of 2,260 calls. The automatic detection algorithm returned a list of 2,161 calls. 2,146 calls were detected correctly, and 15 calls were false positives. Upon closer inspection, 10 out of those 15 false positives were 'one call as two', i.e., a longer call was detected as two short calls. Moreover, 91 calls which were not detected were merged with another close by call, 'two calls as one'. That is, the calls were detected but not as separate calls. An example of "two calls as one" can be seen in the seventh USV in [Figure 4](#). Overall, this results in a recall of 94.9 % and a precision of 99.3 %. To the best of our knowledge, this surpasses the quality measures of other existing USV detection schemes as outlined by Pessoa et al.¹⁰

We also conducted an analysis on how well the algorithm detects the starting and endpoints of the call, which are used for determining the length of the call,

but also for extracting the related snippets of the full recording as input for subsequent classification. On the M-Dataset, on average, the starting point detected by the algorithm was delayed by 0.7 ms and the endpoint was also delayed by an average of 5.2 ms. Hence, when extracting the snippets from the full recording for the classification, we added a suitable padding.

Finally, we ran the algorithm on the full set of 593 recordings, which resulted in a set of more than 160,000 calls.

As experimental settings may vary between institutions, we offer an interactive app that allows users to test and optimize the parameters of the detection algorithm individually.

C. Neural networks for USV classification

Deep learning concepts based on neural networks have become the gold standard for a wide range of classification tasks.²⁰ In the context of USV classifications, where isolated calls are input, it is reasonable to use feed-forward networks.²¹ The two main categories of feed-forward networks are fully connected networks (FNN, multi-layer perceptron) and convolutional networks (CNN). While FNNs inherently possess higher expressive potential, this comes at the expense of a comparatively high number of parameters that must be optimized during the training phase. CNNs, on the other hand, offer an advantage by sharing a small number of coefficients, i.e., they use the same filter weights when mapping an internal layer to a channel of a subsequent layer. This characteristic facilitates the construction of deeper networks with a restricted number of coefficients, hence making CNNs generally more accessible and stable for optimization. However, it is important to note that CNNs operate under the assumption that discriminating features in the input data are shift and scale invariant, a condition that is only partially met in the context of USV data.

For USV data, we can either pre-compute a set of features and feed the resulting feature values into the network for classification. Typical features based on, for example, average energy levels of the USV in certain frequency ranges, are not shift and scale invariant. Hence, a classification based on pre-manufactured features might benefit from an FNN architecture. If we use the full spectrogram as input, we can assume that the individual types of call may shift and scale somewhat arbitrarily in the time-frequency representation of the spectrogram, and a CNN might be advantageous. A disadvantage of using full spectrograms as input is the comparatively high dimension of the input data. Accordingly, we have tested training both types of network with spectrograms of different levels of downsampling as well as training with pre-manufactured feature vectors.

Our experiments using spectrograms of different sizes proved to be superior when compared with feature-based classification schemes. The only feature, which was explicitly used besides the spectrograms, is the duration of the calls.

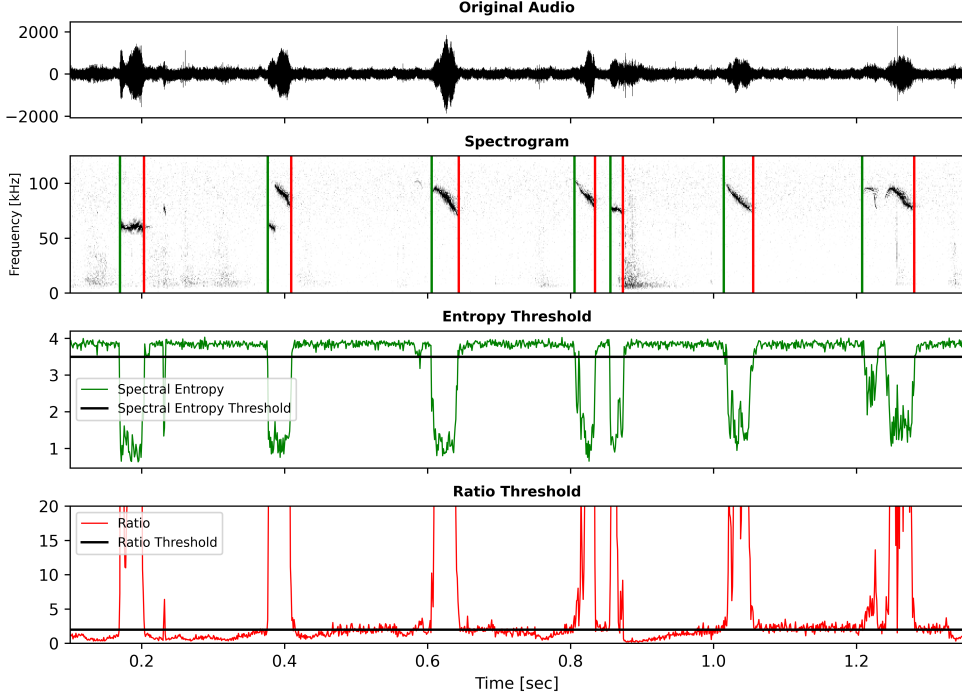


FIG. 4. Example of the detection algorithm with corresponding thresholds.(Color online)

It is pertinent to note that each network necessitates data preprocessing. As is customary, we employed networks with fixed input dimensions, while the extracted USV calls exhibited varying lengths. This presents no issue when utilizing pre-manufactured feature vectors, as the challenge of differing USV lengths is transferred to the computation of feature values. However, when employing a full or downsampled spectrogram as input, the spectrograms of USV calls must first be normalized to a standardized dimension.

1. Fully connected neural networks for USV classification (FNN)

a. Architecture. The network is structured around blocks centered on fully connected layers, each consisting of a batch normalization layer, a fully connected layer, a ReLU activation function, and a dropout layer, see Figure 5. Notably, the initial three blocks exclusively receive the downsampled spectrogram S as input. However, the relative duration information T is integrated into the network in the penultimate layer, effectively forming a Y-shaped architecture. This design artificially increases the importance of the temporal feature.

b. Data Preprocessing. Initially, the USV signals are padded with a duration of 10 ms at the beginning and end to mitigate any potential signal loss during analysis. Subsequently, spectrograms are computed from the padded

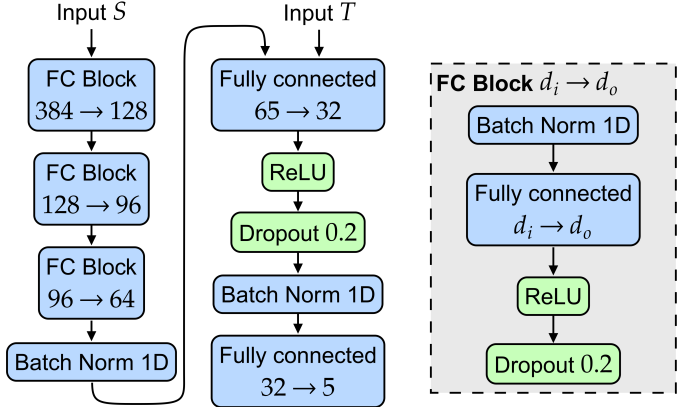


FIG. 5. Network architecture of the FNN used for USV classification.

signals using methods outlined in the detection section, resulting in frequency resolutions of 129 bins. The spectrograms are then converted to a decibel (dB) scale, with a clipping threshold set at 80 dB to control for signal amplification. Notably, the horizontal (time) resolution of the resulting spectrograms varies around an average of 51.4 pixels, with a standard deviation of 24.51 pixels (1 pixel \approx 1 ms). To ensure consistency across samples, the spectrograms are normalized to fall within the range of

$[0, 1]$, utilizing standard min-max normalization:

$$S \leftarrow \frac{S - \min(S)}{\max(S - \min(S))}.$$

During training, the spectrograms are shortened by a random number of pixels ranging from 0 to 9 at the start and end to account for potential inaccuracies in the detected start and end points of the vocalization. Conversely, during testing, spectrograms are shortened by 4 pixels symmetrically, resulting in an effective padding of approximately 6 ms. Following this, spectrograms are resized to a constant resolution of 48×8 pixels.

This resolution was chosen based on a test cycle for different resolutions. For all horizontal resolutions tested, the original vertical resolution of the full spectrogram was set to 129 (the original resolution), and for all vertical resolutions tested, the horizontal resolution was set to 128. Only less than 4 % of our data have an original resolution higher than 128 pixels, making this a valid maximum resolution. Starting from these normalized spectrograms, we then computed down-scaled spectrograms by averaging over neighboring pixels of the spectrogram. As seen in Figure 6, the highest accuracy is achieved for a vertical resolution of 48 pixels and a horizontal resolution of 8. This was flattened into the 1-dimensional feature vector of length 384 and used as the input S .

To normalize sequence lengths, each USV duration is divided by the maximum observed length, which is approximately 150 ms, resulting in the relative duration T . As usual, we randomly add noise to the training data for stabilizing the learning process; we used 5 % additive noise with a normal distribution.

c. Training and Regularization. For training, we use regularization through the use of the Adam optimizer with weight decay, as proposed by Loshchilov and Hutter, with a specific learning rate set at 0.0001.²² To prevent overfitting and promote generalization, a dropout rate of 20 % is applied after each Rectified Linear Unit (ReLU) activation function. The neural network has 71600 trainable parameters.

2. CNN and ViT

In this section we describe the CNN and vision transformer (ViT) architectures, the data preprocessing and the regularization we use for their training.

a. Architectures. The classification experiments using convolutional networks were done with three classical off-the-shelf network architectures (ResNet34²³, ResNet50²³ and EfficientNet-B5²⁴) and a customized architecture based on ResNet blocks. Additionally we used a model with a ViT architecture, ViT-B/16.²⁵

As inspiration for our own customized CNN, we took the paper by He et al., where such an architecture was developed for tasks in computer vision.²³ As can be seen in Table II, our custom CNN is much smaller than off-the-shelf architectures, which is preferable in terms of trainability and interpretability. The specific architecture of the customized CNN can be seen in Figure 7.

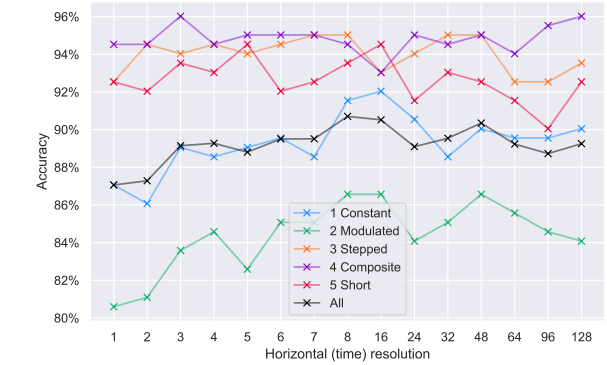
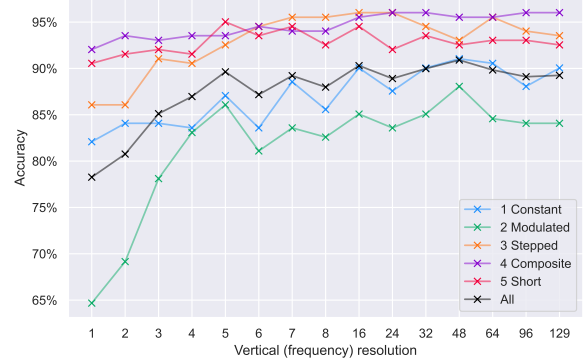


FIG. 6. Evaluation of horizontal (time) and vertical (frequency) resolution. For all horizontal resolutions tested, the vertical resolution was set to 129 (the original resolution) and for all vertical resolutions tested, the horizontal resolution was set to 128. (Color online)

For details on the hardware and software refer to the respective section in the appendix.

b. Data Preprocessing. We adjust the data preprocessing pipeline compared to the one for the FNN model. Since CNNs can handle larger input sizes easier than a fully connected neural network (due to shared parameters), we opt to use the spectrograms at full resolution. Due to batching the data in training, all the spectrograms need to have the same resolution at the end of the pipeline, which we achieve via cropping too long and padding too short spectrograms to the same size. We avoid resizing which would probably make validation more difficult due to the additional distribution shift.

Our data loading and preprocessing pipeline is shown in Figure 8.

The five grey boxes describe transformations only done in the training pipeline (augmentations are only used in training), and the yellow box is only executed in validation phase.

The key features of this preprocessing are as follow. In the first step, we increase the bounds of the signal we obtained from the automatic detection by 60ms on both sides, extending the signal duration before and after the

TABLE II. Number of trainable parameters for the different models.

Model	FNN	Custom CNN	ResNet34	ResNet50	EfficientNet-B5	ViT-B/16
Trainable Parameters	71 600	149 354	21 800 242	25 567 282	30 400 034	85 728 773

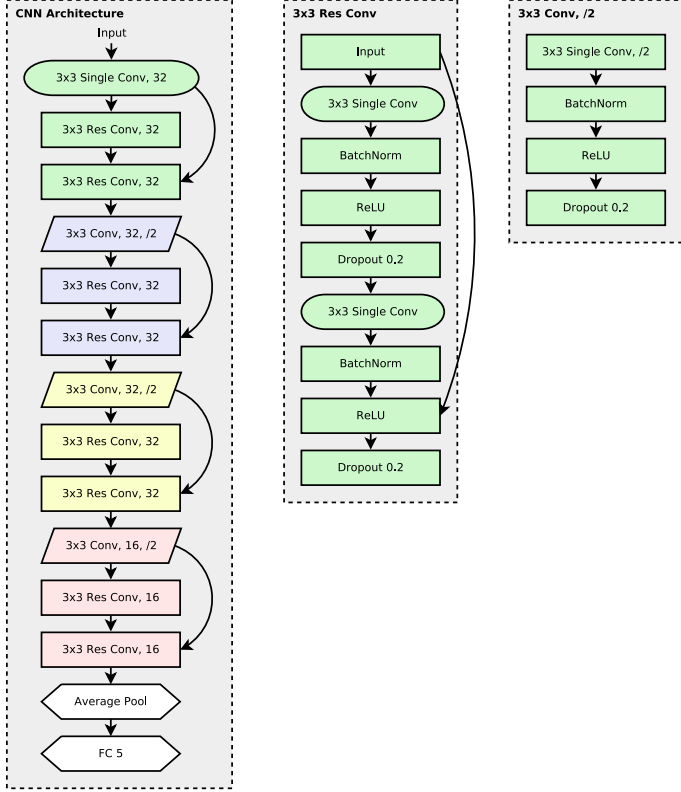


FIG. 7. Model architecture of the custom CNN.

detected signal (this is to compensate for the random shift). Then we transform the signal into a 2d spectrogram, and use both the original spectrogram and a spectrogram rescaled to a decibel scale (while clipping its lower end so that the whole spectrogram has a 60 dB range). Both spectrograms are concatenated, i.e. merged into a single data block, and used as input for the network. In order to improve robustness and to avoid overfitting, we then randomly translate the spectrograms by up to 10ms on the time axis as augmentation in the training cycle (we do not want the model to overfit on the position of the call, since the detection boundaries can vary).

As previously mentioned, due to batching the data in training all spectrograms need to be transformed into the same shape. We do this by determining the midpoint in time of the spectrograms and by extracting the central part of the spectrograms, i.e. the data is center cropped to $\min(\ell - 100, 170)$ with ℓ being the duration of the spectrograms in milliseconds (crop too long spec-

trograms to a maximum size of 170). Then we subtract the mean and divide by the standard deviation of the labeled dataset to normalize the data. After that we use replication padding to pad the spectrograms to a length of 190 ms, at this point all spectrograms have the same shape of $2 \times 201 \times 190$, as required for batching.

For the validation of the pipeline, the spectrograms are only center cropped to a length of 170, thus completing the pipeline. For the training pipeline, we use additional data augmentations, to improve robustness and to avoid overfitting. We rescale the spectrograms on the time axis randomly between 170 ms and 220 ms, center crop them to 150 ms, randomly translate them by -10 to 10 on the frequency axis and finally add gaussian noise with a standard deviation of 0.01.

Before we output the spectrograms, we stack the time feature into them as an additional channel (replicate the time feature value over all spatial positions), resulting in a final spectrogram shape of $3 \times 201 \times 170$ for validation, respectively $3 \times 201 \times 150$ for training.

c. Training and Regularization. For regularization, we use Adam with weight decay with the default learning rate of 0.001 as optimizer.²² Further we use label smoothing in the loss (we use 0.05 and 0.9 as targets instead of 0.0 and 1.0). For the custom CNN, we additionally use twenty percent dropout after each activation function. Meaning that for each element there is a 20 % chance that the value is set to zero.²⁶ For the other models, we use their default settings, which means no dropout in ResNet34, ResNet50 and ViT and stochastic dropout of resnet blocks in EfficientNet-B5 with a maximum probability of 0.2 (which gets linearly scaled by the layer of the model, so for a given layer the dropout probability would be $0.2 \cdot \frac{\text{layer id}}{\text{number of layers}}$). The stochastic dropout in the EfficientNet-B5 model works for each row of the batch, i.e. an entire input is zeroed out.

IV. RESULTS

For the presentation of our results we distinguish between the fully automated and the semi-automated case. The fully automated setting refers to the scenario where a set of USV recordings is provided as input, and a list of individual calls along with their classifications is returned. This case is presented in the next subsection. On the other hand, the semi-automated case aims to reduce the manual workload and to achieve a desired recall, typically higher than what is achievable with the fully automated setting. In the semi-automated setting, we require an additional measure that evaluates the quality of

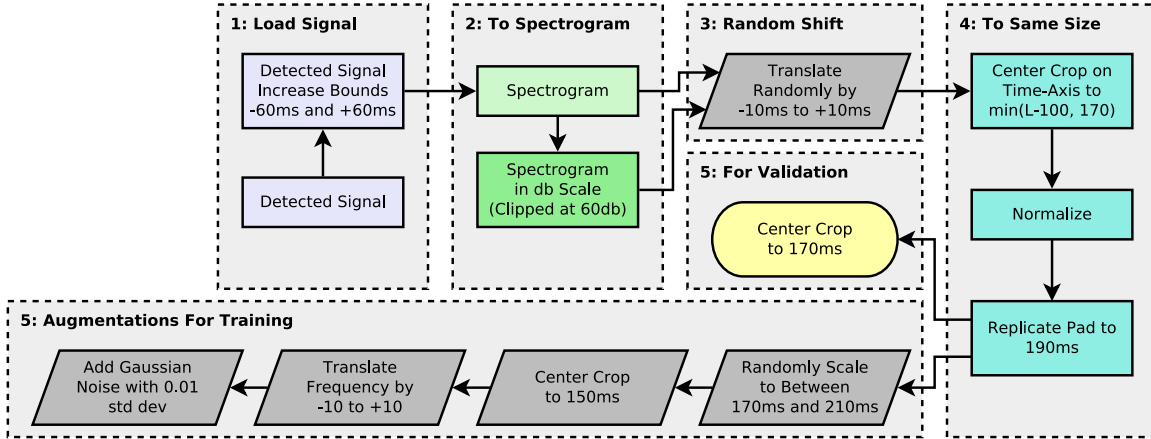


FIG. 8. Data loading pipeline for the CNNs and ViT.

the classification result. Depending on this quality measure, the system either returns the classification result or retains the particular call for further manual inspection.

In the following subsection, we focus on the results of the classification step. The results of the detection step were already presented in section III B.

A. Evaluation metrics for classification

The quality of the different neural network architectures for the classification of neonatal USV calls are based on 10-fold cross-validation with A-data set plus using the whole M-data set for training. The A-data set is randomly split into 10 disjunct splits (all neural network architectures use the same 10 splits) with the union of those 10 splits resulting in the whole A-data set. Then we train 10 models (per network architecture), each time using 9 splits for training and 1 split for validation, where we choose a different validation split for each of the 10 models. The reported quality measures are averaged over those 10 models.

The usual quality measures (accuracy, recall, precision, specificity, F1-score) are computed for either class-wise classification or for determining an overall score. For class-wise classification we treat our multi-class problem as a binary-class problem, we determine the quality measures in a one vs all manner, i.e. for each class we treat all the other classes as the same class. E.g. true positive refers to the number of calls, that were correctly assigned to this class, true negatives refer to all calls not in this class which were assigned to any of the other classes, similar for false positives and false negatives. We then use

the standard definitions:

$$\begin{aligned}
 \text{Accuracy} &= \frac{\text{True Positives} + \text{True Negatives}}{\text{All}} \\
 \text{Recall} &= \frac{\text{True Positives}}{\text{True Positives} + \text{False Negatives}} \\
 \text{Specificity} &= \frac{\text{True Negatives}}{\text{True Negatives} + \text{False Positives}} \\
 \text{Precision} &= \frac{\text{True Positives}}{\text{True Positives} + \text{False Positives}} \\
 \text{F1-score} &= 2 \cdot \frac{\text{Precision} \cdot \text{Recall}}{\text{Precision} + \text{Recall}}
 \end{aligned}$$

The recall focuses on capturing all actual positive instances, while the specificity focuses on correctly identifying all actual negative instances. The precision penalizes false positives and the F1-score is a measure for the balance of precision and recall.

We compute the overall accuracy as the ratio between correct predictions and all predictions, as previously described.^{10,27} For the other values, we compute them per class in a one vs all manner, and report the weighted mean over the classes, as described in Pessoa et al.¹⁰ In a multi-class setting, the class weighted binary recall results in the ratio of correct predictions to all predictions, i.e. for multi-class our reported recall is the same as the reported accuracy. The results are given in percent.

B. Fully automated classification

In the following section, we will compare the performance of the FNN, the Custom CNN (with different variants of preprocessing and downsampling), the ResNet34, ResNet50, EfficiencyNet-B5 and the ViT. The mentioned networks differ in their architecture and also in their size, see Table II). A (*) next to the model name indicates that the smooth spectrograms were normalized individually in the data preprocessing pipeline (i.e. the mean of each smooth spectrogram gets set to 0 and the

standard deviation to 1), as opposed to normalizing them over the global mean and standard deviation of all the smooth spectrograms in the M-data set.

As already mentioned, we use tenfold cross-validation on the A-data set for evaluation. Hence, for each network architecture, we trained ten models, and evaluated them separately. For class-wise evaluation for each of the these models we compute accuracy, precision, recall, specificity and F1-score all binary in a one-vs-all approach. The global numbers reported for precision, recall, specificity and F1-score are then the weighted sums over all five classes, i.e. we weight the quality measures for each class by the number of samples in this class and sum them up. These values are averaged over all ten runs of the cross-validation, which also allows us to compute the variance over these ten runs. The global recall is the ratio of correct predictions to all predictions. The results are displayed in [Table III](#). We note a few observations before going into more detail on the performance of the custom CNN. The EfficientNet-B5 model performs best, but with more than 30 million trainable parameters it is also the largest of the convolutional models we used. The vision transformer (ViT-B/16) does not perform well, which is expected due to the low amount of data we have for training (vision transformer generally require larger amounts of training data compared to CNNs, in the original paper they were pretrained on a dataset consisting of 300 million images, whereas we only have 4374 spectrograms for training).²⁵ For ViT-B/16, we rescaled the spectrograms to a final size of 160x160, as the image size needs to be a multiple of the patch size (16). The custom CNN performed similar to the EfficientNet-B5 with only 149,000 trainable parameters, therefore for the following interpretability section we focus on the custom CNN model.

For the custom CNN we add the results for some variants. E.g. the use of data augmentations and regularization in the model, gives us an increase of 3.92 % in recall (in [III](#) 'Custom CNN no aug reg' uses no augmentation or regularization and has 3.92 % lower recall than the original model). Additionally, downsampling the spectrogram to 25×8 drastically reduces performance ('Custom CNN 25×8 '), hence we decided to work with full spectrograms for classification with all CNNs. Not clipping dB values in the spectrograms ('Custom CNN no dB limit') did slightly increase performance measures but at the expense of a higher variance, therefore we included dB clipping. Also, duplicate channels did not yield a better performance ('Custom CNN $\times 2$ channels'). Hence, we fixed the custom CNN network as described in the previous section. The performance is presented in [Table III](#). For a class-wise evalution of the cutom CNN see [Table IV](#). Detailed information on the FNN can be seen in [Table V](#).

C. Semi-automated USV analysis

Alternative to the fully-automated approach one can use the last layer of the network, which gives a pseudo-

probability for each of the five classes, as a quality indicator to sort out calls where the algorithm is not sure. Allowing the user to define a threshold $p \in [0, 1]$ and accept the algorithms finding only, if the algorithmic pseudo-probability exceeds p for at least one class. For each value of p , we determine the number of calls reaching pseudo-probabilities above the threshold and report the resulting recall.

We have plotted the resulting curves in [Figure 9](#). I.e. for the EfficientNet-B5 model a threshold of $p = 0.8$ allows to classify 71.7 % of the calls with an recall of 92.5 %. As described, we were aiming for the 80 – 90 challenge, i.e. we aspired to classify 80 % of all calls automatically with a recall of at least 90 %.

To further examine the effects of limiting the evaluation to samples, for which the neural network outputs a relatively high confidence, we developed the graphic shown in [Figure 9](#). First, let us focus on the histograms, shown in red and green with their values represented on the left-hand y-axis. For a total of 21 equally spaced confidence intervals, we calculate the relative amount of samples, with a prediction confidence falling into the given interval. This is done for correctly and wrongly classified samples separately. It is evident that most correctly classified samples have a high confidence and vice versa for the wrongly classified calls.

This motivates a confidence dependent evaluation of the neural network, which represents a generalization of the before mentioned 80 – 90 challenge. To visualize this, we plot the recall (solid blue line) and the amount of data preserved (dashed blue line) in dependence of the pseudo-probability p . For example, if all samples with a prediction confidence of less than 0.6 are omitted, 81.7 % of the data is left, for which the network reaches a recall of 83.5 %.

In summary, the proposed data analysis pipeline is capable of selecting and classifying 82.7 % of all calls with a recall of 90.4 % (with a threshold of $p = 0.7$). The remaining calls are separated and can be analyzed manually. In total, this allows an almost arbitrarily high recall while still saving a substantial time of manual labor.

D. Interpretability of the Custom CNN

In this section, we aim to analyze how the classification network reaches its decisions. We start by displaying channel visualizations of the different layers, followed by saliency maps that highlight which parts of the input the model relies on for its prediction.

1. Channel Visualization

Channel visualizations indicate which structures are analyzed at different channels. These visualizations serve as basic building blocks, and the output values of these channels can be interpreted as a measure of how strongly the input correlates with these structures. A description of how the visualizations are computed can be found in the appendix. For example, [Figure 10](#) displays several channels that are tuned for analyzing constant, increas-

TABLE III. Results of the classification models, evaluated on the 10 fold cross validation test data.

Model	Precision	Specificity	F1 Score	Accuracy
FNN	78.14 ± 2.48	90.49 ± 1.14	77.14 ± 2.61	77.35 ± 2.55
Custom CNN	87.02 ± 1.46	94.68 ± 1.21	86.69 ± 1.46	86.79 ± 1.45
Custom CNN no aug reg	83.28 ± 1.62	93.09 ± 1.79	82.37 ± 2.00	82.86 ± 1.75
Custom CNN no db limit	87.24 ± 2.71	94.80 ± 1.40	87.76 ± 2.80	86.88 ± 2.71
Custom CNN 25x8	70.03 ± 2.64	85.60 ± 1.87	68.75 ± 2.34	70.09 ± 1.94
Custom CNN x2 channels	86.81 ± 1.62	94.69 ± 0.92	86.41 ± 1.69	86.49 ± 1.61
ResNet34 (*)	86.75 ± 1.24	94.64 ± 1.10	86.21 ± 1.42	86.34 ± 1.39
ResNet50 (*)	87.27 ± 1.51	94.86 ± 0.11	86.80 ± 1.43	86.88 ± 1.55
EfficientNet B5 (*)	87.58 ± 1.43	95.27 ± 0.07	87.21 ± 1.35	87.28 ± 1.36
Custom CNN (*)	86.10 ± 1.46	94.34 ± 1.00	85.67 ± 1.33	85.84 ± 1.35
ViT-B/16 (*)	57.75 ± 4.30	76.45 ± 2.89	55.84 ± 3.20	61.89 ± 2.38

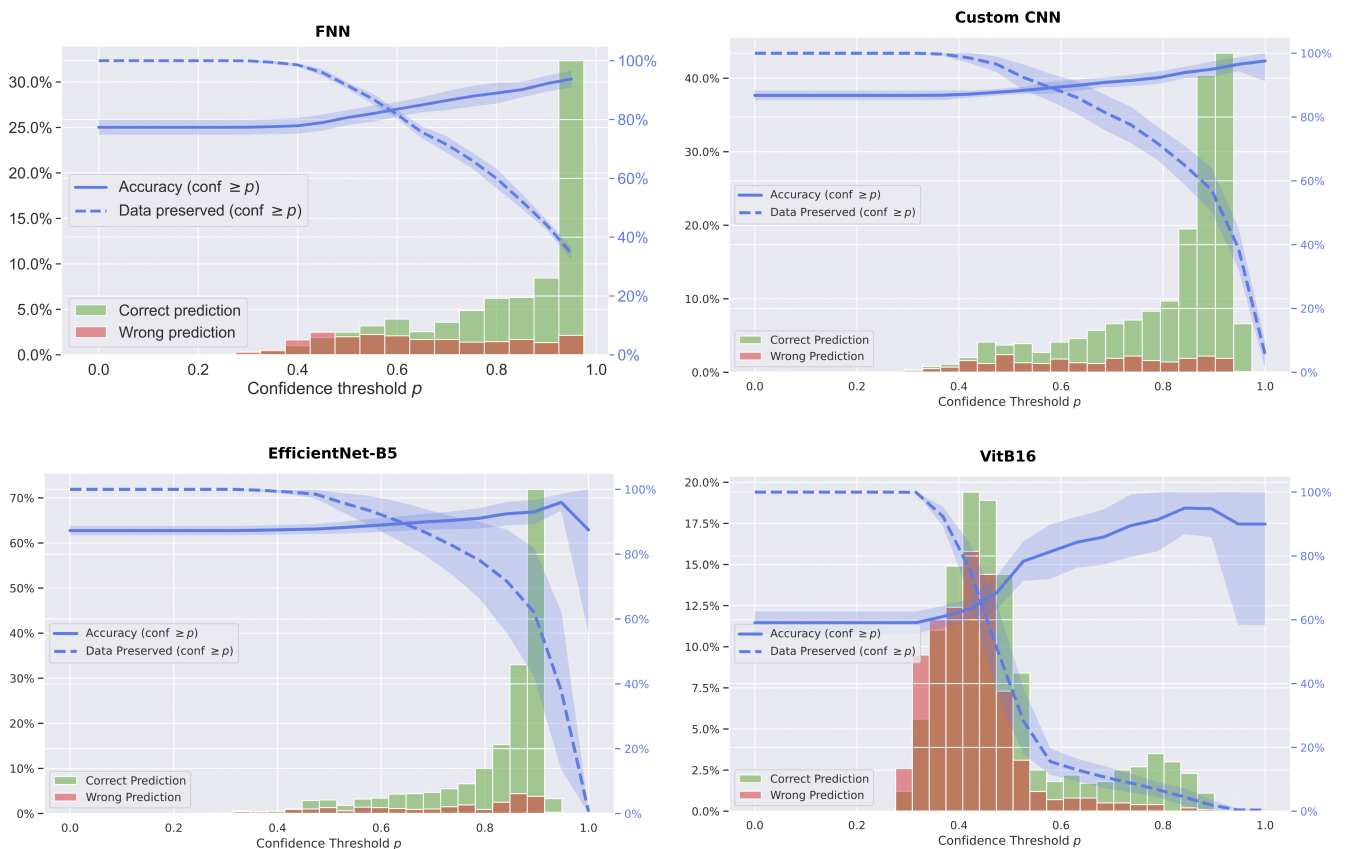


FIG. 9. Mean and standard deviation of the recall on the validation data of the 10-fold cross validation sets while ignoring the predictions with the lowest confidence. (Color online)

ing, or decreasing frequency content. The channel at the bottom left seems to capture signals with a discontinuity in frequency. The multiplicity of similar channels might indicate that similar results could be achieved with a smaller network. However, these similar structures are

combined with different follow-up structures in the subsequent layers, so this multiplicity is necessary for allowing a subtle analysis.

The structures in the channel visualizations of the later layers become increasingly difficult to analyze. The

TABLE IV. Results of the custom CNN model shown per class, evaluated on the 10 fold cross validation test data. All the metrics (including Accuracy) in the Table are computed in a one vs all manner.

Class	Precision	Recall	Specificity	F1 Score	Accuracy
1	78.07 ± 5.68	80.14 ± 9.93	96.50 ± 1.41	78.77 ± 5.63	94.39 ± 1.75
2	89.41 ± 3.13	91.68 ± 3.49	91.36 ± 3.00	90.45 ± 1.61	91.55 ± 1.37
3	85.17 ± 5.84	79.73 ± 7.82	97.47 ± 1.32	82.14 ± 5.38	94.83 ± 1.65
4	86.05 ± 9.58	75.56 ± 8.09	98.75 ± 1.19	80.00 ± 6.23	96.92 ± 1.19
5	89.39 ± 3.25	89.51 ± 5.01	97.39 ± 0.78	89.37 ± 3.10	95.88 ± 0.97

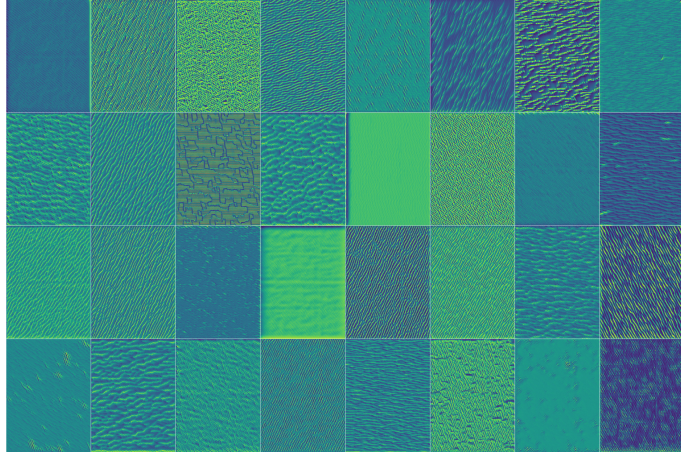


FIG. 10. Visualisation of the activations in the 32 channels of the first layer of the network.

channel visualizations for all layers of the network are depicted in [section X](#).

2. Saliency Maps

As a second approach for explaining how the network functions, we used saliency maps which are computed as follows. For a given input one determines how strongly every pixel contributes towards the final classification.

As method to generate the saliency map, we use Integrated Gradients²⁸ combined with SmoothGrad²⁹. For details, refer to the appendix.

As examples, we plot the saliency maps for prototypical vocalizations for every class, see [Figure 11](#). As expected, a well trained network looks at the prototypical shapes of the signal and focuses on the main frequencies at each time instant. It neglects e.g. the blurring in frequency and the background structures almost completely. We take this as a confirmation that the network is well trained for the task at hand.

V. DISCUSSION

In this paper, we have developed two neural network architectures (FNN, custom CNN) for USV classification

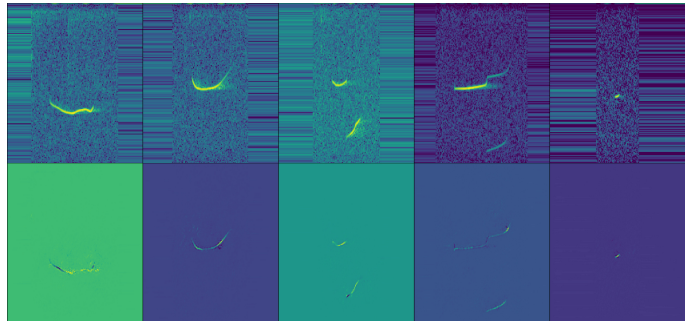


FIG. 11. Top row: input data for calls from different classes, the effect of the padding structure for normalizing the inputs to fixed dimensions are visible; bottom row: The resulting saliency maps show that the network indeed is looking at core structures of the signals and neglects the noise background. The calls classes are: constant, modulated, frequency step, composite and short call in that respective order.

and we compared them with much larger off-the-shelf network architectures (several CNNs, Visual Transformer ViT). The best results in terms of overall accuracy were achieved by the 'EfficientNet B5' architecture. However, ResNet50 as well as our custom CNN achieve a comparable accuracy which is within the range of 0.5 % of EfficientNet B5.

Alternative architectures, such as ViT and FNN, did not achieve comparable performance levels. The reasons for these inferior results vary. ViT, a large and powerful architecture, demands vast quantities of training data. In the present setting, overfitting to the relatively limited training data is nearly inevitable, hindering further improvements in training. As for FNN, we posit that the inherent but constrained translation invariance of the classification task, wherein slight shifts in signal frequency or timing do not alter classification outcomes, provides convolutional network architectures with a distinct advantage.

Among the top architectures (EfficientNet B5, ResNet 50, custom CNN), we employ two additional criteria to determine the optimal network architecture for USV classification. Firstly, the variance observed across ten cross-validation runs provides insight into the robustness of each architecture. In this regard, both EfficientNet B5 and our custom CNN demonstrate superior stability and minimal variance. Secondly, we evaluate the potential for semi-automated classification. Both architectures achieve approximately 89 % classification accuracy with over 90 % precision. Consequently, EfficientNet B5 and the custom CNN yield comparable results. In conclusion, EfficientNet B5 and custom CNN achieve comparable results. Hence, we favor the smaller network, due to its more transparent architectures and the comparatively modest training times. In summary, our results indicate, that CNNs with residual connections are a good architecture for this type of data and we would recommend our custom CNN for further research.

Let us comment on some further design decisions. We did extensive experiments with subsampled spectrograms, which lead to some conclusions, that we did not expect at the beginning. E.g. the FNN architectures allows a rather coarse subsampling without loosing accuracy, indeed best results were achieved with a downsampling to 48×8 spectrograms.

Results were not so drastic for the custom CNN, but also here a rather coarse downsampling in the time variable is acceptable. In contrast, we need a fine discretization in frequency. As an explanation, we assume that different USVs may differ slightly in their dominant frequencies, but the structure of the calls does not vary significantly over its duration. Hence, we need a fine discretization in frequency, but a downsampling in time does not hamper the quality of classification. As an explanation why downsampling is critical for CNNs, let us have a look at the saliency maps. This reveals that the CNN looks at the 'skeleton' of the calls, i.e. at the very fine central line in the spectrogram, this is much harder to detect in blurred and downsampled signal.

Also, the decision to separate detection and classification tasks can be questioned. However, this separation followed standard procedure and allows for a separate, focused analysis of the unique challenges in each task. For instance, the data preprocessing requirements differ significantly. Our refined preprocessing pipeline, particularly tailored for the CNN network, emphasizes the critical nature of this initial step.

In addition, we would like to comment on some failed approaches. As already mentioned, we experimented with classification schemes reliant on hand-crafted feature vectors. Specifically, we adopted feature vectors utilized in.¹⁰ However, juvenile USVs are constantly evolving, making it harder to classify them using predefined parameters. Despite efforts to enhance the feature vectors by incorporating additional metrics like energy level ratios, we were unable to achieve accuracies surpassing 80 %.

We also observed that preprocessing of the data is crucial. The presented results were obtained after substantial testing of the different preprocessing steps.

Training of the networks, as described, used standard concepts such as Adam, but substantial tests runs were needed before finding the optimal setup for the optimization strategy. This was done by trial and error.

Naturally, the presented study on deep learning concepts for USV classification is not complete. There are other recent concepts, which would be worthwhile to explore in this context. E.g. networks including attention mechanisms or contrastive learning for pre-clustering the USV data or recurrent networks, which would allow to feed in the full USV recording and get directly to a classification without a preliminary detection step are all rather novel and potentially advantages concepts. In this sense, our approach of comparing feed forward networks either based on the classical FNN or on CNN concepts is only a natural first step in the direction of developing optimal algorithms for the task at hand.

VI. CONCLUSION

The presented research is part of a larger investigation, which aims at evaluating the phenotype of three mouse lines with suspected autism-like behavior. As the manual analysis of the full dataset (593 recordings) would have required more than half a year of rather tiring routine work by a skilled expert, the goal was to develop an automated pipeline capable of detecting and classifying USVs. The presented results demonstrate that indeed such an automated analysis is possible in a completely automated setup with a classification accuracy of 86.79 %.

If this level of accuracy is deemed insufficient, we have outlined a procedure to assess the confidence of the classification. This enables us to establish a subset that can be automatically classified with even greater accuracy, thereby significantly reducing the manual effort required to analyze the original dataset.

We also evaluated whether the AI focuses on the essential aspects of the spectrogram and have provided visual explanations of the classification patterns.

More importantly, we successfully demonstrated the quantitative and qualitative efficacy of our fully automated pipeline within a research context. In the recordings from our autism-like mouse lines examined in this study, our pipeline revealed significant quantitative differences between wildtype and mutant mice. Specifically, as illustrated in [Figure 12](#), mutated animals exhibited considerably fewer vocalizations at P4 compared to their wildtype littermates (no difference was detected at P8 and P12). The detection algorithm not only demonstrated high reliability, but also processed a dataset beyond the analytical capacity of a human evaluator.

Moreover, the combined approach of detection and classification enabled us to uncover qualitative differences, such as distinct distributions of calls per class, at developmental stages (P8 and P12) where quantitative analysis alone failed to identify a phenotype, see [Figure 13](#) and [Figure 14](#) for details. Given demonstrated capability of the pipeline to analyze subtle differences in pup USVs on a large scale, we will implement the algorithm for further USV analysis at the INBC in Heidelberg.

Over the process of this paper, we have tested different deep learning models in order to analyse which architecture is best for analyzing USVs. For future endeavors we are open to collaborating with other research teams tackling similar tasks in USV classification, thus broadening the scope of the proposed pipeline. We have indicated various avenues where emerging AI concepts like contrastive learning or attention mechanisms could enhance detailed analysis, though the necessity for such advancements remains to be seen. Additionally, we are keen on integrating expert knowledge, such as MEL diagrams, which adjust the frequency scale according to mice perception, potentially enabling further refinement in analysis.

Furthermore, we anticipate that our work will enrich the understanding of both the capabilities and constraints of AI in practical data analysis.

VII. SUPPLEMENTARY MATERIAL

ACKNOWLEDGMENTS

R. Herdt is funded by the Deutsche Forschungsgemeinschaft (DFG, German Research Foundation) - project number 459360854.

VIII. AUTHOR DECLARATIONS

The authors have no conflicts of interest to declare. This study was approved by the Governmental Council Karlsruhe (Project Number G172/21). The co-authors Herdt, Kinzel, Maass and Walther contributed equally to this work. The authors Maass and Schaaf are the last authors.

IX. DATA AVAILABILITY

The data that support the findings of this study are openly available in [repository name] at [http://doi.org/\[doi\]](http://doi.org/[doi]), reference number [reference number].

X. APPENDIXES

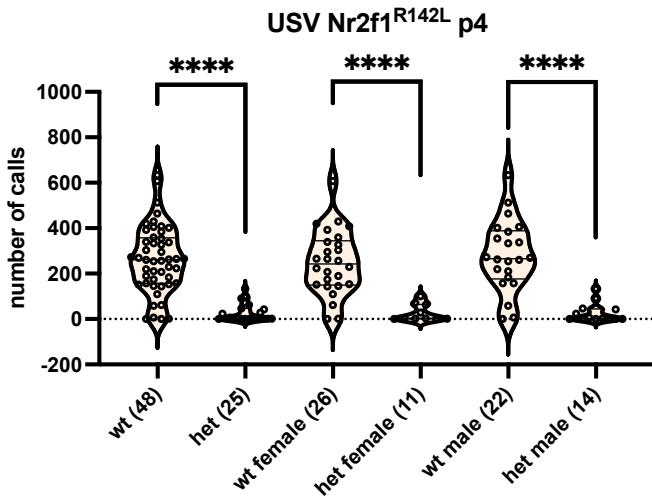


FIG. 12. Quantitative differences in call number at P4 as detected by our segmentation algorithm.

A. Channel Visualization

First we compute the channel visualizations of the different layers. These visualizations are computed by activation maximization³⁰ while utilizing transformation robustness as in³¹.

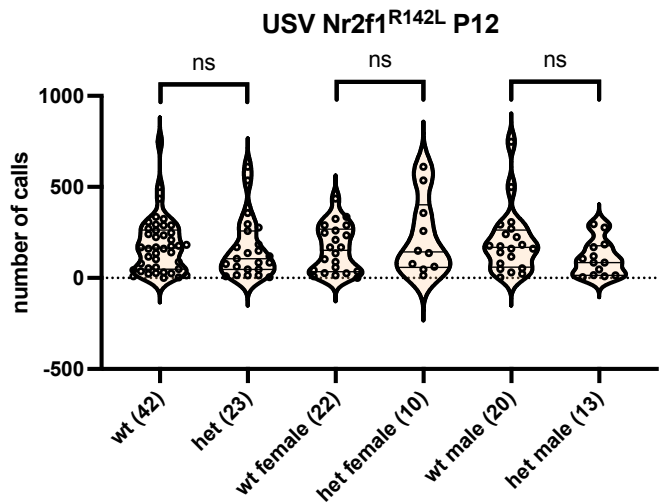


FIG. 13. No quantitative differences in the call number at P12, as detected by our segmentation algorithm.

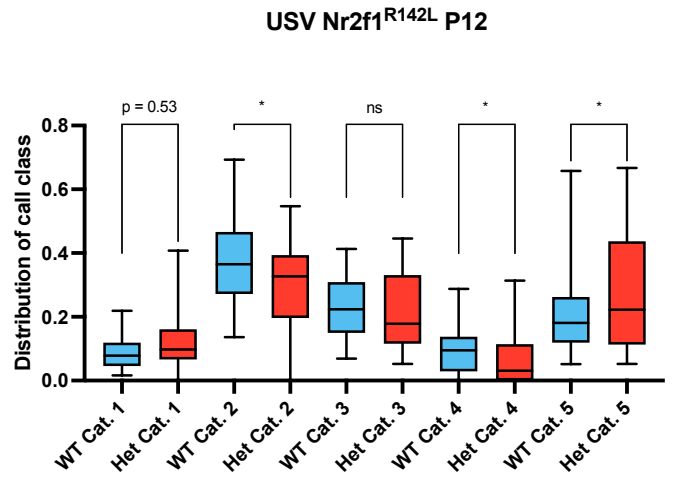


FIG. 14. Qualitative differences in the call categories at P12, as detected by our classification algorithm.

We synthesize those channel visualizations using iterative gradient descent, as shown in Figure 1. As optimizer we use Adam with a learning rate of 0.05.³² We start from random gaussian noise, and then iteratively update the image $z^{(i)}$ to maximize activation of the channel c . To reduce noise and make the visualizations more interpretable, we use transformation robustness as in.³¹ This is depicted by the function g in (*) in 1. We randomly move the image by up to one pixel and randomly scale it between 0.9 and 1.1. One problem with the generation of those visualizations is getting stuck in the initial initialization, if the initial image is not activating the channel c (the channel c being zero everywhere and

TABLE V. Results of the FNN shown per class, evaluated on the 10 fold cross validation test data.

Class	Precision	Recall	Specificity	F1 score	Accuracy
all	78.14 ± 2.48	77.35 ± 2.55	90.49 ± 1.14	77.14 ± 2.61	88.75 ± 1.23
1	60.38 ± 7.98	63.41 ± 6.65	93.60 ± 2.25	61.58 ± 6.69	89.67 ± 2.45
2	80.36 ± 3.62	84.76 ± 4.26	83.95 ± 2.65	82.40 ± 2.66	84.25 ± 1.98
3	76.10 ± 9.14	65.99 ± 8.33	96.30 ± 1.62	70.47 ± 7.75	91.80 ± 1.97
4	89.05 ± 7.72	57.49 ± 11.60	99.46 ± 0.34	69.39 ± 10.17	96.03 ± 1.28
5	79.48 ± 6.84	86.90 ± 2.50	94.52 ± 1.80	82.82 ± 3.39	92.95 ± 1.18

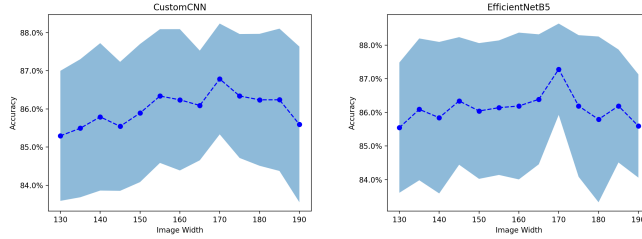


FIG. 15. Mean accuracy on the validation data of the 10 fold cross validation sets over the duration in ms of the spectrograms. For both the custom CNN and the EfficientNet-B5 the maximum accuracy of 86.79 respectively 87.28 is reached at a size of 170(ms), whereas the training size was 150(ms).

therefore the gradient being zero and the image will never update). To avoid this problem, for the first 16 iterations we change the backward pass of the final ReLU layer in F_X to directly return the incoming gradient (i.e. we allow the gradient backwards even if the activation was zero in the forward pass). Also we only optimize the spectrogram, we keep the time feature fixed at the mean time of all the calls.

B. Additional Saliency maps

We use five samples in SmoothGrad with a noise of standard deviation of 0.1 and 50 samples in Integrated Gradients. This means, we run Integrated Gradients five times, each time adding random noise with a standard deviation of 0.1 to the image, and return the mean of the five runs as the saliency map.

In Figure 11 we only plot the dB scale spectrogram, and the saliency map for it, and ignore the smooth spectrogram. This is due to the insight from Table VI, which shows that the model does not rely on the smooth spec-

TABLE VI. Accuracy of the custom CNN when 'removing' inputs, evaluated on the 10 fold cross validation test data.

Model	Original	Remove smooth spec	Time feature to avg	Remove db spec
Accuracy	86.79 ± 1.45	86.54 ± 1.52	82.76 ± 2.19	38.91 ± 11.88

ALGORITHM 1: Visualize channel c from layer X of the model.

Input: model from layers 0 to X F_X
 $z^{(0)} \sim \mathcal{N}(0, 0.05)$
for $i \leftarrow 0$ to n **do**
 $\text{loss} \leftarrow \nabla_{z^{(i)}}[F_X(g(z^{(i)}))]_c$ (*)
 backpropagate loss
 update $z^{(i)}$
end for

rogram for its prediction, but only on the dB scale spectrogram and somewhat on the time feature.

C. Hardware and Software

For the implementations of the neural networks we use the pytorch library, and for setting up multi-GPU training we use the [pytorch-lightning](#) library.³³ To compute the saliency maps for interpreting the custom CNN we use the implementations of the captum library.³⁴ We use the implementation of the [torchvision library](#) for the architectures of the ResNet34, ResNet50, EfficientNet-B5²⁴ and ViT-B/16²⁵. For the ResNet34, ResNet50 and EfficientNet-B5 we adjust the final fully connected layer (we input the time feature as an additional channel there). All our experiments regarding the CNNs and the ViT were conducted on a Linux server with 8 Nvidia RTX 2080Ti GPUs. The experiments for the FNN were conducted on Windows with GTX 1080.

XI. REFS

- 1 C. V. Portfors, "Types and functions of ultrasonic vocalizations in laboratory rats and mice," *J. Am. Assoc. Lab. Anim. Sci.* **46**(1), 28–34 (2007).
- 2 T. Peleh, A. Eltokhi, and C. Pitzer, "Longitudinal analysis of ultrasonic vocalizations in mice from infancy to adolescence: Insights into the vocal repertoire of three wild-type strains in two different social contexts," *PLoS One* **14**(7), e0220238 (2019).
- 3 M. L. Scattoni, S. U. Gandhy, L. Ricceri, and J. N. Crawley, "Unusual repertoire of vocalizations in the BTBR T+tf/J mouse model of autism," *PLoS One* **3**(8), e3067 (2008).
- 4 R. W. Elwood and F. Keeling, "Temporal organization of ultrasonic vocalizations in infant mice," *Dev. Psychobiol.* **15**(3), 221–227 (1982).
- 5 E. Ey, N. Torquet, A.-M. Le Sourd, C. S. Leblond, T. M. Boeckers, P. Faure, and T. Bourgeron, "The autism ProSAP1/Shank2 mouse model displays quantitative and structural abnormalities in ultrasonic vocalisations," *Behav. Brain Res.* **256**, 677–689 (2013).
- 6 M. L. Scattoni, J. Crawley, and L. Ricceri, "Ultrasonic vocalizations: a tool for behavioural phenotyping of mouse models of neurodevelopmental disorders," *Neurosci. Biobehav. Rev.* **33**(4), 508–515 (2009).
- 7 D. M. Holtzman, D. Santucci, J. Kilbridge, J. Chua-Couzens, D. J. Fontana, S. E. Daniels, R. M. Johnson, K. Chen, Y. Sun, E. Carlson, E. Alleva, C. J. Epstein, and W. C. Mobley, "Developmental abnormalities and age-related neurodegeneration in a mouse model of down syndrome," *Proc. Natl. Acad. Sci. U. S. A.* **93**(23), 13333–13338 (1996).
- 8 A. Dirks, E. W. Fish, T. Kikusui, J. van der Gugten, L. Groenink, B. Olivier, and K. A. Miczek, "Effects of corticotropin-releasing

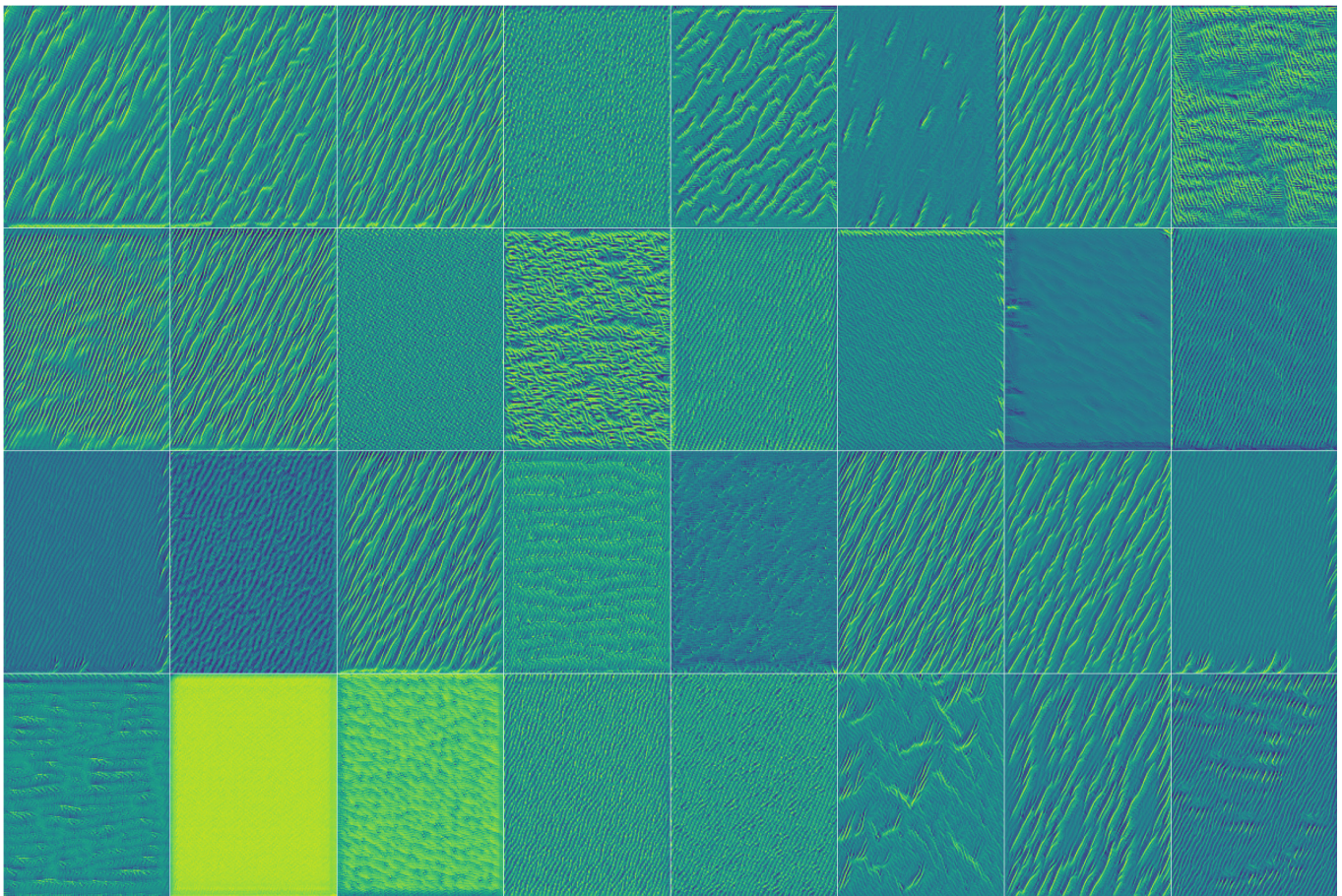


FIG. 16.

hormone on distress vocalizations and locomotion in maternally separated mouse pups,” *Pharmacol. Biochem. Behav.* **72**(4), 993–999 (2002).

⁹K. R. Coffey, R. E. Marx, and J. F. Neumaier, “DeepSqueak: a deep learning-based system for detection and analysis of ultrasonic vocalizations,” *Neuropsychopharmacology* **44**(5), 859–868 (2019).

¹⁰D. Pessoa, L. Petrella, P. Martins, M. Castelo-Branco, and C. Teixeira, “Automatic segmentation and classification of mice ultrasonic vocalizations,” *J. Acoust. Soc. Am.* **152**(1), 266 (2022).

¹¹T. Takumi, K. Tamada, F. Hatanaka, N. Nakai, and P. F. Bolton, “Behavioral neuroscience of autism,” *Neurosci. Biobehav. Rev.* **110**, 60–76 (2020).

¹²G. Ehret, “Infant rodent ultrasounds – a gate to the understanding of sound communication,” *Behav. Genet.* **35**(1), 19–29 (2005).

¹³Y. Goussha, K. Bar, S. Netser, L. Cohen, Y. Hel-Or, and S. Wagner, “HybridMouse: A hybrid Convolutional-Recurrent neural Network-Based model for identification of mouse ultrasonic vocalizations,” *Front. Behav. Neurosci.* **15**, 810590 (2021).

¹⁴F. de Chaumont, N. Lemièvre, S. Coqueran, T. Bourgeron, and E. Ey, “LMT USV toolbox, a novel methodological approach to place mouse ultrasonic vocalizations in their behavioral Contexts-A study in female and male C57BL/6J mice and in shank3 mutant females,” *Front. Behav. Neurosci.* **15**, 735920 (2021).

¹⁵A. H. Fonseca, G. M. Santana, G. M. Bosque Ortiz, S. Bampi, and M. O. Dietrich, “Analysis of ultrasonic vocalizations from

mice using computer vision and machine learning,” *Elife* **10** (2021).

¹⁶S. Bonzano, I. Crisci, A. Podlesny-Drabiniok, C. Rolando, W. Krezel, M. Studer, and S. De Marchis, “Neuron-Astroglia cell fate decision in the adult mouse hippocampal neurogenic niche is Cell-Intrinsically controlled by COUP-TFI in vivo,” *Cell Rep.* **24**(2), 329–341 (2018).

¹⁷M. Bertacchi, C. Tocco, C. P. Schaaf, and M. Studer, “Pathophysiological heterogeneity of the BBSOA neurodevelopmental syndrome,” *Cells* **11**(8) (2022).

¹⁸J. M. S. Grimsley, J. J. M. Monaghan, and J. J. Wenstrup, “Development of social vocalizations in mice,” *PLoS One* **6**(3), e17460 (2011).

¹⁹A. Oppenheim, R. Schafer, and J. Buck, *Discrete-time signal processing* (Prentice Hall, 1999).

²⁰C. C. Aggarwal, *Neural Networks and Deep Learning: A Textbook*, 1st ed. (Springer Publishing Company, Incorporated, 2018).

²¹A. M. da Silva and P. Sussner, “A brief review and comparison of feedforward morphological neural networks with applications to classification,” in *Artificial Neural Networks - ICANN 2008, 18th International Conference, Prague, Czech Republic, September 3–6, 2008, Proceedings, Part II*, edited by V. Kurková, R. Neruda, and J. Koutník, Springer (2008), Vol. 5164 of *Lecture Notes in Computer Science*, pp. 783–792, https://doi.org/10.1007/978-3-540-87559-8_81, doi: [10.1007/978-3-540-87559-8_81](https://doi.org/10.1007/978-3-540-87559-8_81).

²²I. Loshchilov and F. Hutter, “Decoupled weight decay regularization” (2019).

²³K. He, X. Zhang, S. Ren, and J. Sun, “Deep residual learning for image recognition,” in *2016 IEEE Conference on Computer*

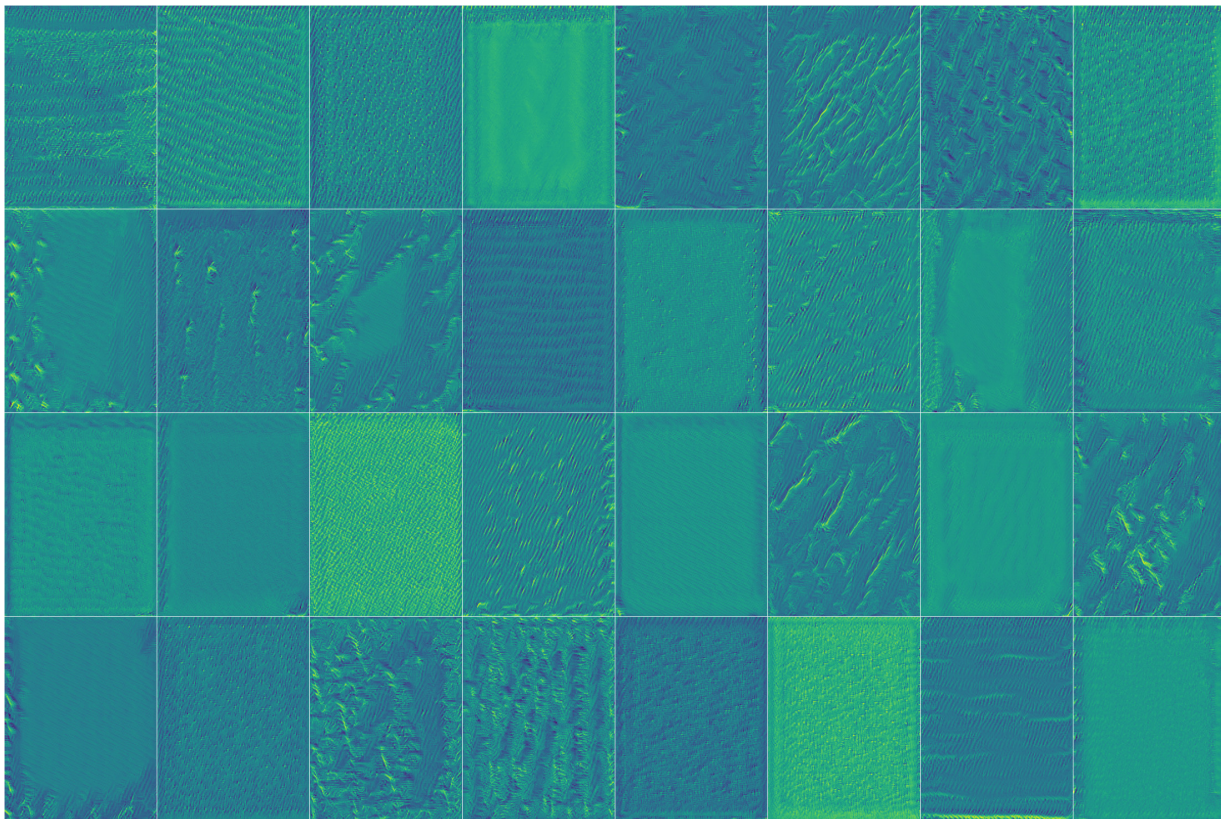


FIG. 17.

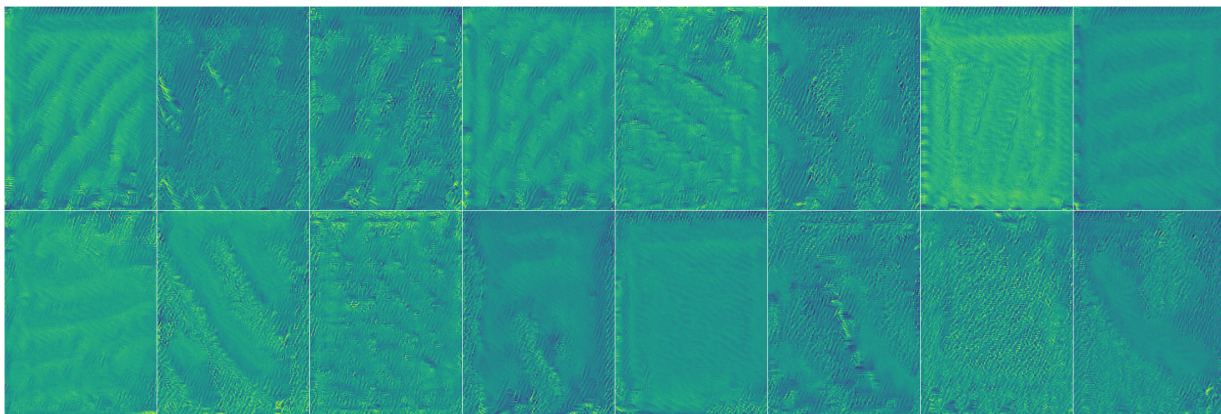


FIG. 18.

Vision and Pattern Recognition (CVPR) (2016), pp. 770–778, doi: [10.1109/CVPR.2016.90](https://doi.org/10.1109/CVPR.2016.90).

²⁴M. Tan and Q. Le, “EfficientNet: Rethinking model scaling for convolutional neural networks,” in *Proceedings of the 36th International Conference on Machine Learning*, edited by K. Chaudhuri and R. Salakhutdinov, PMLR (2019), Vol. 97 of *Proceedings of Machine Learning Research*, pp. 6105–6114, <https://proceedings.mlr.press/v97/tan19a.html>.

²⁵A. Dosovitskiy, L. Beyer, A. Kolesnikov, D. Weissenborn, X. Zhai, T. Unterthiner, M. Dehghani, M. Minderer, G. Heigold, S. Gelly, J. Uszkoreit, and N. Houlsby, “An image is worth 16x16 words: Transformers for image recognition at scale,” in *9th International Conference on Learning Representations, ICLR 2021, Virtual Event, Austria, May 3–7, 2021, OpenReview.net (2021)*, <https://openreview.net/forum?id=YicbFdNTTy>.

national Conference on Learning Representations, ICLR 2021, Virtual Event, Austria, May 3–7, 2021, OpenReview.net (2021), <https://openreview.net/forum?id=YicbFdNTTy>.

²⁶N. Srivastava, G. Hinton, A. Krizhevsky, I. Sutskever, and R. Salakhutdinov, “Dropout: A simple way to prevent neural networks from overfitting,” *Journal of Machine Learning Research* **15**(56), 1929–1958 (2014) <http://jmlr.org/papers/v15/srivastava14a.html>.

²⁷A. H. Fonseca, G. M. Santana, G. M. Bosque Ortiz, S. Bampi, and M. O. Dietrich, “Analysis of ultrasonic vocalizations from mice using computer vision and machine learning,” *eLife* **10**, e59161 (2021) <https://doi.org/10.7554/eLife.59161> doi: [10.7554/eLife.59161](https://doi.org/10.7554/eLife.59161).

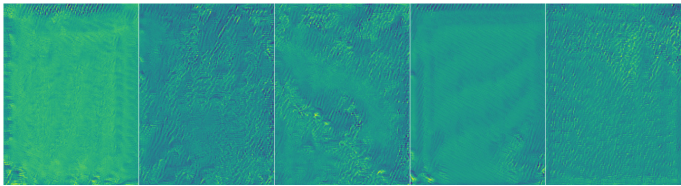


FIG. 19.

7554/eLife.59161.

²⁸M. Sundararajan, A. Taly, and Q. Yan, “Axiomatic attribution for deep networks,” in *Proceedings of the 34th International Conference on Machine Learning*, edited by D. Precup and Y. W. Teh, PMLR (2017), Vol. 70 of *Proceedings of Machine Learning Research*, pp. 3319–3328, <https://proceedings.mlr.press/v70/sundararajan17a.html>.

²⁹D. Smilkov, N. Thorat, B. Kim, F. Viégas, and M. Wattenberg, “Smoothgrad: removing noise by adding noise” (2017), <https://arxiv.org/abs/1706.03825>, doi: [10.48550/ARXIV.1706.03825](https://doi.org/10.48550/ARXIV.1706.03825).

³⁰D. Erhan, Y. Bengio, A. Courville, and P. Vincent, “Visualizing higher-layer features of a deep network,” Technical Report, Université de Montréal (2009).

³¹C. Olah, A. Mordvintsev, and L. Schubert, “Feature visualization,” *Distill* (2017) doi: [10.23915/distill.00007](https://doi.org/10.23915/distill.00007) <https://distill.pub/2017/feature-visualization>.

³²D. P. Kingma and J. Ba, “Adam: A Method for Stochastic Optimization,” in *3rd International Conference on Learning Representations, ICLR 2015, San Diego, CA, USA, May 7-9, 2015, Conference Track Proceedings* (2015).

³³A. Paszke, S. Gross, F. Massa, A. Lerer, J. Bradbury, G. Chanan, T. Killeen, Z. Lin, N. Gimelshein, L. Antiga, A. Desmaison, A. Kopf, E. Z. Yang, Z. DeVito, M. Raison, A. Tejani, S. Chilamkurthy, B. Steiner, L. Fang, J. Bai, and S. Chintala, “Pytorch: An imperative style, high-performance deep learning library,” in *Advances in Neural Information Processing Systems 32: Annual Conference on Neural Information Processing Systems 2019, NeurIPS 2019, December 8-14, 2019, Vancouver, BC, Canada*, edited by H. M. Wallach, H. Larochelle, A. Beygelzimer, F. d’Alché-Buc, E. B. Fox, and R. Garnett (2019), pp. 8024–8035, <https://proceedings.neurips.cc/paper/2019/hash/bdbca288fee7f92f2bfa9f7012727740-Abstract.html>.

³⁴N. Kokhlikyan, V. Miglani, M. Martin, E. Wang, B. Alsallakh, J. Reynolds, A. Melnikov, N. Kliushkina, C. Araya, S. Yan, and O. Reblitz-Richardson, “Captum: A unified and generic model interpretability library for pytorch” (2020).